

1 ~~Large Ozone Intrusions during Sudden Stratospheric Warmings Enhance~~  
2 ~~Ozone Radiative Forcing Over South Asia~~

3 **Large Ozone Enhancement over South Asia Triggered by Sudden**  
4 **Stratospheric Warming under Westerly QBO phase: Implications on**  
5 **Ozone Radiative Forcing**

6 Shubhajyoti Roy<sup>1,2</sup>, Satheesh Chandran PR<sup>1</sup>, Suvarna Fadnavis<sup>1\*</sup>, Vijay Sagar<sup>1</sup>, Michaela I.  
7 Hegglin<sup>3,4,5</sup>, Rolf Müller<sup>3</sup>, Prashant Chavan<sup>1</sup>

8 <sup>1</sup>Indian Institute of Tropical Meteorology, Centre for Climate Change Research, India

9 <sup>2</sup>Department of Atmospheric and Space Sciences, Savitribai Phule Pune University, Pune, India

10 <sup>3</sup>Institute of Energy and Climate Systems: Stratosphere (ICE-4), Forschungszentrum Jülich,  
11 Jülich, Germany

12 <sup>4</sup>Institute for Atmospheric and Environmental Research, University of Wuppertal, Wuppertal,  
13 Germany

14 <sup>5</sup>Department of Meteorology, University of Reading, Reading, United Kingdom

15 \*Corresponding author email: [suvarna@tropmet.res.in](mailto:suvarna@tropmet.res.in)

16

17

18

## 19 Abstract

20 Tropospheric ozone pollution in South Asia is mainly blamed on anthropogenic emissions.  
21 However, based on ERA5 reanalysis data, this study highlights the contribution of stratospheric  
22 ozone intrusions into the Upper Troposphere and Lower Stratosphere (UTLS) associated with  
23 Sudden Stratospheric Warming (SSW) events in enhancing upper tropospheric ozone over the  
24 South Asian region. We report an enhancement in ozone in the UTLS by more than 80% for  
25 2018 and ~30% within  $\pm 6$  days of the onset during SSW events concurrent with the westerly  
26 phase of ~~the QBO~~ Quasi-biennial oscillation (WQBO-SSW) compared to non-SSW years. The  
27 equatorward shift (south of  $30^{\circ}\text{N}$ ) of the subtropical jet during WQBO-SSW causes ~~deepening~~  
28 ~~lowering~~ of the tropopause and ~~more~~ Rossby-wave ~~penetration~~ breaking in the upper  
29 troposphere. This results in higher ~~Rossby-wave-breaking-and~~ stratospheric ozone intrusions over  
30 the South Asian region. The ozone enhancement during WQBO-SSW events produces an  
31 instantaneous radiative forcing at the top of the atmosphere of  $0.09 \pm 0.05 \text{ W.m}^{-2}$  due to UTLS  
32 ozone changes and  $0.17 \pm 0.05 \text{ W.m}^{-2}$  from total-column ozone changes over South Asia. ~~The~~  
33 ~~elevated tropospheric ozone levels resulting from stratospheric intrusions pose a threat to humans~~  
34 ~~and vegetation.~~

35 Keywords: Sudden stratospheric warming, stratosphere intrusions, ozone radiative forcing, South  
36 Asian region, Rossby wave breaking.

## 37 1. Introduction

38 Tropospheric ozone is a short-lived greenhouse gas that plays a crucial role in  
39 atmospheric chemistry and radiative forcing (Wang et al., 2022). It is also a major air pollutant  
40 that significantly affects human health (Lim et al., 2012; Fleming et al., 2018), damages

41 vegetation (~~Fowler et al., 2009~~; Feng et al., 2021), disrupts ecosystems, and imposes economic  
42 costs (Dewan and Lakhani, 2022). In South Asia, a significant amount of tropospheric ozone is a  
43 growing concern due to its increased hazardous health effects (~~Silva et al., 2013~~; Lin et al.,  
44 2018).

45         The contribution from the downward transport of ozone-rich air from the stratosphere is  
46 the largest natural source of tropospheric ozone (e.g., Fadnavis et al., 2010; Roy et al., 2020).  
47 Studies have reported that stratospheric influence on the tropospheric ozone exceeds 50% in the  
48 winter season at the extratropics (Williams et al., 2019). Wang and Fu (2021) estimate that  
49 stratosphere-to-troposphere exchange (STE) contributes approximately  $347 \pm 12$  Tg year<sup>-1</sup> to the  
50 global tropospheric ozone budget based on both observations and reanalysis data. CMIP6 model  
51 simulations for the period 1997 to 2014 indicate that up to 30% of surface ozone in the Northern  
52 Hemisphere during winter (DJF) is due to stratospheric ozone intrusions (Li et al., 2024). In the  
53 Northwest Pacific, STE increases mid and upper-tropospheric ozone by about 96% in winter and  
54 40% in summer between 1990 and 2020 (Ma et al., 2024). Roy et al. (2023) reported an ozone  
55 enhancement of ~40 ppb in the upper troposphere over the Indian region caused by stratospheric  
56 intrusions associated with tropical cyclones.

57         Sudden stratospheric warming (SSW) events play a key role in atmospheric dynamics  
58 and stratospheric ozone intrusions into the troposphere (e.g., Williams et al., 2024). SSWs are  
59 one of the most significant large-scale dynamical phenomena in the stratosphere during winter  
60 (Butler et al., 2015; ~~de la Cámara et al., 2018~~; Baldwin et al., 2021). Enhanced planetary wave  
61 activity from the troposphere disrupts the stratospheric polar vortex, decelerating or even  
62 reversing the stratospheric westerlies, and causing a rapid rise in polar stratospheric temperatures  
63 by up to 50 K within few days (Baldwin et al., 2021). SSW events are crucial in modulating

64 extreme heat, air pollution, wildfires, wind extremes, storm clusters, tropical cyclones, and sea  
65 ice melt in the northern high latitudes (Domeisen and Butler, 2020; Domeisen et al., 2020). The  
66 temperature and wind anomalies associated with SSWs propagate downward into the  
67 troposphere over timescales ranging from weeks to months, impacting tropospheric weather in  
68 the Northern Hemisphere for up to 40 days following the onset of the event (Baldwin and  
69 Dunkerton, 2001; Hall et al., 2021). Studies also suggest that SSWs are often followed by an  
70 equatorward shift of the tropospheric jet stream and storm tracks, as well as surface pressure  
71 anomalies that resemble the negative phase of the Northern Annular Mode (Sigmond et al., 2013;  
72 Kidston et al., 2015). Projection studies suggest that SSW events will increase by approximately  
73 one event per decade by the end of the 21<sup>st</sup> century (Charlton-Perez et al., 2008). High  
74 greenhouse gas emission scenarios indicate a doubling in SSW frequency (Schimanke et al.,  
75 2012). Considering the frequent occurrences and the potential role of SSWs in STE, it is  
76 important to investigate SSWs influence on tropospheric ozone enhancements and the associated  
77 radiative effects.

78 SSW events have a significant influence on STE and impact the tropospheric ozone  
79 budget, particularly in high-latitude regions (Xia et al., 2023; Williams et al., 2024; Lee et al.,  
80 2025). Based on 11 polar-night jet oscillation (PJO) type SSW events from 1980 to 2013 and  
81 chemistry-climate model simulations, STE led to an average increase of 5–10% in near-surface  
82 ozone over the Arctic (Williams et al., 2024). Xia et al. (2023) reported an even more  
83 pronounced increase of 76% in Arctic surface ozone due to STE in the 2020/21 SSW event.  
84 While most of these studies focus on the polar regions, some have identified SSW-induced ozone  
85 variability in the mid-latitudes (Liu et al., 2009; ~~Lu et al., 2022~~; Williams et al., 2024). ~~For~~  
86 ~~example, Lu et al. (2022) demonstrated that meteorological changes associated with SSWs cause~~

87 ~~poor air quality in the Beijing-Tianjin-Hebei region.~~ Liu et al. (2009) noted an ozone  
88 enhancement of about 186 Tg in the upper troposphere over East Asia during the 2002–2003  
89 SSW, using MOZART-3 simulations. However, tropospheric ozone variations during SSW  
90 events over South Asia are among the least studied. Additionally, the broader implications of  
91 these events on the ozone radiative forcing over this region remain largely underexplored.

92 In this study, we investigate the impact of all the SSW events from 1962 to 2018 on  
93 ozone variability in the upper troposphere and lower stratosphere (UTLS: 300-50 hPa) over the  
94 South Asian region (20-35°N, 65-90°E) using ERA5 reanalysis data. The composite is obtained  
95 by averaging data with the onset day as a central date (details in the ‘Methods’ section). ~~Here, we~~  
96 ~~report a significant ozone enhancement in the UTLS over South Asia, leading to increased ozone~~  
97 ~~radiative forcing. All SSWs were examined during the period from 1962 to 2018. This revealed~~  
98 ~~more equatorward shift of the subtropical jet over South Asia (~23°N) and associated large~~  
99 ~~ozone intrusion in this region during the 2018 SSW relative to other SSW years. This motivated~~  
100 ~~us to report the detailed mechanism of the 2018 SSW as a case study.~~ A recent study by Shi et al.  
101 (2023) ~~reported that during~~ reports the influence of the 2018 SSW over East Asia, surface  
102 temperatures dropped by up to ~18°C relative to pre-event conditions ~~causing anomalous cooling~~  
103 ~~of 18°C.~~ However, to our knowledge, UTLS ozone responses over South Asia during this event  
104 have received limited attention, which motivates our emphasis on the 2018 case. We further  
105 extend the analysis to all SSWs and assess their contribution to upper-tropospheric ozone and  
106 regional ozone radiative forcing.

107 The paper is organised as follows. Section 2 describes the ERA5 reanalysis dataset, and  
108 the computation of ozone radiative forcing using the radiative-kernel method. Section 3 presents

109 the (i) UTLS ozone changes during the 2018 SSW event over South Asia, (ii) composite analysis  
110 of SSWs, and (iii) ozone radiative forcing. Section 4 summarises the main findings.

## 111 **2. Methods**

### 112 **2.1 ERA 5 Reanalysis Data**

113 We analysed daily data of ozone, zonal and meridional winds, geopotential height (GPH),  
114 and potential vorticity (PV) from the fifth-generation reanalysis dataset (ERA5) provided by the  
115 European Centre for Medium-Range Weather Forecasts (ECMWF) (Hersbach et al., 2020). The  
116 ERA5 ozone field is generated through assimilation of multiple satellite- and ground-based  
117 observations, including TOMS (1978–2006), SBUV v8.6 (1978–present), CCI MIPAS (2005–  
118 2012), SCIAMACHY (2002–2012), Aura MLS v4.2 (2004–present), and OMI-DOAS (2004–  
119 present) (Hersbach et al., 2020; S-RIP Final Report, 2022). Comparison of ERA5 ozone with  
120 observations shows a slight overestimation in the UTLS. For example, over the North India  
121 region, ERA5 shows an overestimation of ~20 ppb ozone (Fadnavis et al., 2023). [However,](#)  
122 [ERA5 ozone showed lesser biases compared to other reanalyses \(Fadnavis et al., 2023\).](#) The S-  
123 RIP (2022) assessment report states an overestimation [of zonal mean ozone by ~10–40%](#)  
124 [between 50°N and 50°S. Overall, ERA5 ozone shows lesser biases than other reanalyses](#)  
125 [\(Fadnavis et al., 2023\). We analysed ERA5 ozone, geopotential height, winds, and potential](#)  
126 [vorticity \(PV\) data for this study.](#) The ERA5 variables have a horizontal resolution of  $0.25^\circ \times$   
127  $0.25^\circ$  across 37 standard pressure levels (1000 to 1 hPa). Composite analysis is conducted for all  
128 variables for  $\pm 30$  days, centered on the onset of SSW events (30 days before and after the onset),  
129 to assess the impact.

130 Daily anomalies in ozone, geopotential height, winds, and PV during the SSW days were  
131 calculated by subtracting the corresponding calendar-day climatology, computed from all the

132 non-SSW years. The long-term trend is removed from the daily ERA5 data before computing  
133 anomalies. This approach ensures that anomalies reflect deviations from typical background  
134 conditions. To determine statistical significance, we used the Monte Carlo bootstrap and the  
135 Wilcoxon signed-rank test. For the Monte Carlo, we built a calendar-matched ~~null~~non-SSW  
136 background ensemble by resampling days from non-SSW years within the same day-of-year  
137 window (20,000 resamples). We then use a bias-corrected and accelerated (BCa) bootstrap with  
138 20,000 resamples to form 95% confidence intervals. For 2018, we checked whether the observed  
139 value lay outside the BCa interval of the background ensemble. For the composite, we computed  
140 the event composite mean and tested it against the distribution of composite means obtained  
141 from the same non-SSW background ensemble (20,000 resamples). ~~whether the mean anomaly~~  
142 ~~differed from zero~~. A grid point was considered significant if the event composite mean lay  
143 outside the 95% BCa confidence interval of this background distribution. Next, we applied an  
144 exact Wilcoxon signed-rank test to the same data. A grid point is called significant only when  
145 both tests agree at 95% significance.

146 The onset of all the 2018 SSW events is identified as the day when the zonal mean  
147 westerly winds at 10 hPa and 60°N reverse their direction from westerlies to easterlies (Charlton  
148 and Polvani 2007). Figure S1 shows the temporal evolution of the zonal-mean zonal wind at 60°  
149 N and 10 hPa for the 2018 SSW event. To diagnose stratospheric intrusions, we use potential  
150 vorticity (PV) as a dynamical tracer of stratospheric air and adopt the 2-PVU contour as a proxy  
151 for the dynamical tropopause (e.g., Kunz et al., 2011; Holton et al., 1995). Intrusions are  
152 identified from PV streamers or tropopause folds when high-PV ( $\geq 2$  PVU) extends equatorward  
153 and downward into the upper troposphere (e.g., Sprenger et al., 2007) ~~associated for Rossby-~~  
154 ~~wave breaking (RWB) in the upper troposphere. A PV value greater than 2 PVU in the upper~~

155 ~~troposphere is taken as an indicator of a stratospheric intrusion (e.g., Holton et al., 1995; Stohl et~~  
156 ~~al., 2003).~~ To demarcate the boundary between the troposphere and stratosphere, we used the  
157 WMO lapse-rate tropopause (WMO 1997). We used the lapse rate tropopause (LRT) derived  
158 from the ERA5 data for the present study (Hoffmann and Spand 2022). This definition is adopted  
159 to mark a temporally varying troposphere–stratosphere boundary that is consistent with the  
160 dynamical changes. Further, phases of the Quasi-biennial oscillation (QBO) are identified using  
161 zonal-mean zonal wind data from radiosonde observations published by the Freie Universität  
162 Berlin. The classification of westerly and easterly QBO phases is based on winds at 70 hPa.  
163 Periods with positive zonal wind values ( $>0 \text{ m.s}^{-1}$ ) are identified as the westerly QBO (WQBO),  
164 while periods with negative zonal wind values ( $<0 \text{ m.s}^{-1}$ ) are classified as the easterly QBO  
165 (EQBO).

## 166 **2.2 Computation of ozone radiative forcing**

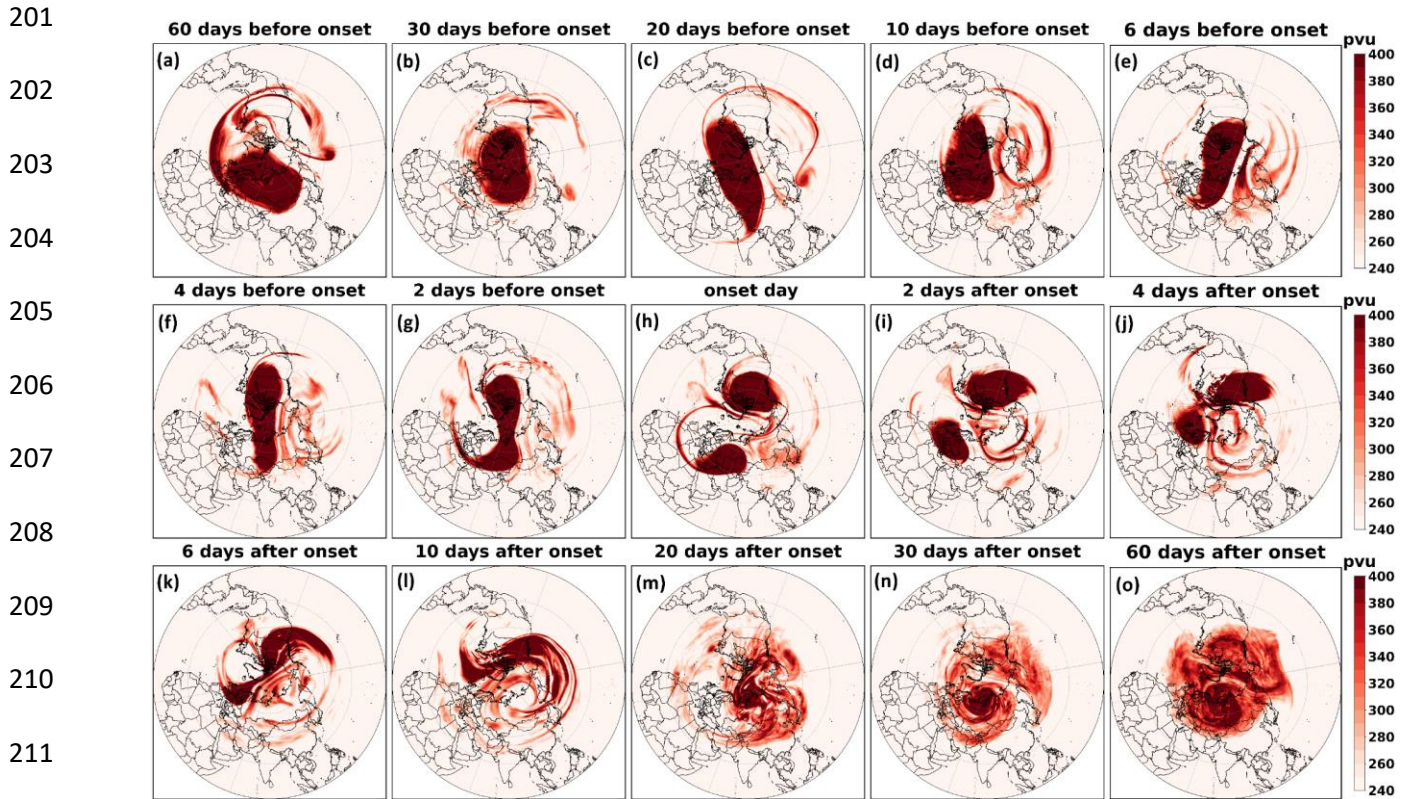
167 The ozone radiative forcing (RF) is estimated using an ozone radiative kernel method  
168 (Skeie et al., 2020). The radiative kernel is constructed using the University of Oslo radiative  
169 transfer model (Myhre et al., 2011) by perturbing the ozone layer-by-layer. Temperature, water  
170 vapour, and clouds are incorporated into the model from ECMWF's forecast for the year 2003  
171 and applied as monthly averages. The model calculates radiative forcing using a broad-band  
172 scheme for longwave radiation (Myhre and Stordal, 1997) and the DIScrete Ordinate Radiative  
173 Transfer (DISORT) code for shortwave radiation (Stamnes et al., 1988). Previous studies have  
174 shown that the ozone radiative forcing estimates from the radiative kernel technique and a  
175 radiative transfer model agree within  $0.01 \text{ W.m}^{-2}$  globally (Iglesias-Suarez et al., 2018). Before  
176 applying the kernel, the ERA5 ozone data are linearly interpolated to the kernel resolution ( $\sim 5.6^\circ$   
177  $\times 5.6^\circ$  horizontal, with 60 vertical levels). The interpolated ozone fields are first converted into

178 layer-wise partial column amounts in Dobson units (DU) following Ziemke et al. (2001). Ozone  
179 anomalies in DU are then computed from the non-SSW climatology at each grid point. These  
180 layer wise DU anomalies are multiplied by the long-wave instantaneous clear-sky ozone kernel  
181 ( $\text{W}\cdot\text{m}^{-2}\cdot\text{DU}^{-1}$ ), which gives the change in top-of-atmosphere (TOA) long-wave radiative flux  
182 (defined as an increase in net downward flux;  $\Delta (F_{\text{in}} - F_{\text{out}}) > 0$ ) per DU of ozone change in  
183 each layer. Following Shell et al. (2008), we calculate the instantaneous ozone RF by vertically  
184 summing the layer wise TOA contributions from the UTLS and the total atmosphere.

### 185 **3. Results**

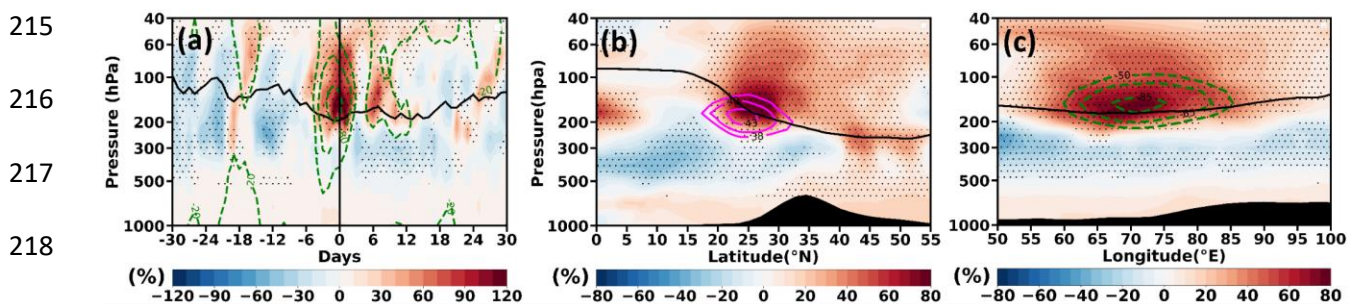
#### 186 **3.1 Polar vortex evaluation in 2018 SSW event**

187 The time evolution of the vortex structure depicted by PV at 10 hPa for  $\pm 30$  days around  
188 the 2018 SSW onset is shown in Fig. 1. As the SSW event approaches, the vortex begins to  
189 elongate and become asymmetrical (Fig. 1a-g) due to the influence of planetary wave activity  
190 propagating upward from the troposphere; such deformation of the vortex was reported in the  
191 past (e.g., Baldwin et al., 2021). On the onset day (12 February), the vortex splits into two high-  
192 PV lobes, one positioned over North America and another over Eurasia (Fig. 1h). Following the  
193 onset, smaller vortices exhibit swirling and filamentation, with the Eurasian lobe drifting  
194 westward (Fig. 1i-j). Polar vortex splitting or deformations cause equatorward meandering of  
195 upper tropospheric jet that affect the Rossby wave breaking (RWB) and ozone intrusions in the  
196 mid-latitudes (Baldwin et al., 2021; Albers et al., 2015; ~~Gomez-Escolar et al., 2014~~). The  
197 equatorial meandering of the jet may influence the tropical region; however such analysis is  
198 sparse. In the following sections we show the influence of the 2018 SSW on the South Asian  
199 region. First we show ozone variation in the UTLS over South Asia and then explain the  
200 associated dynamical changes in RWB and the upper tropospheric jet.



212 **Figure 1.** Time slice of the spatial distribution of potential vorticity (PV) at 10 hPa from 30 days  
213 before to 30 days after the onset of the 2018 SSW event.

214 **3.2 February 2018 SSW case: UTLS ozone variation**



219 **Figure 2.** (a) Temporal evolution of vertical ozone anomalies averaged over the South Asian  
220 region (65-90°E, 20-35°N) from 30 days before to 30 days after the onset for the 2018 event. (b)  
221 Latitude-pressure section of ozone anomalies averaged over South Asia (65 - 90°E) for  $\pm 6$  days  
222 around the onset for 2018 SSW event. (c) is the same as that of (b) but represents longitude  
223 variations of vertical ozone anomalies averaged over South Asia (20-35°N). The **horizontal and**  
224 **the vertical solid black line** in (a) represent **380 K potential temperature isoline and** the onset  
225 **day, respectively**. Magenta solid contour lines in (b) represent the mean zonal wind and green  
226 dashed contour lines in (a) and (c) represent the GPH anomaly. Solid black lines in panels (b-c)  
227 (a-c) represent the lapse rate tropopause. Black dots indicate a region of 95% confidence level.  
228 (Figure created using Python software).

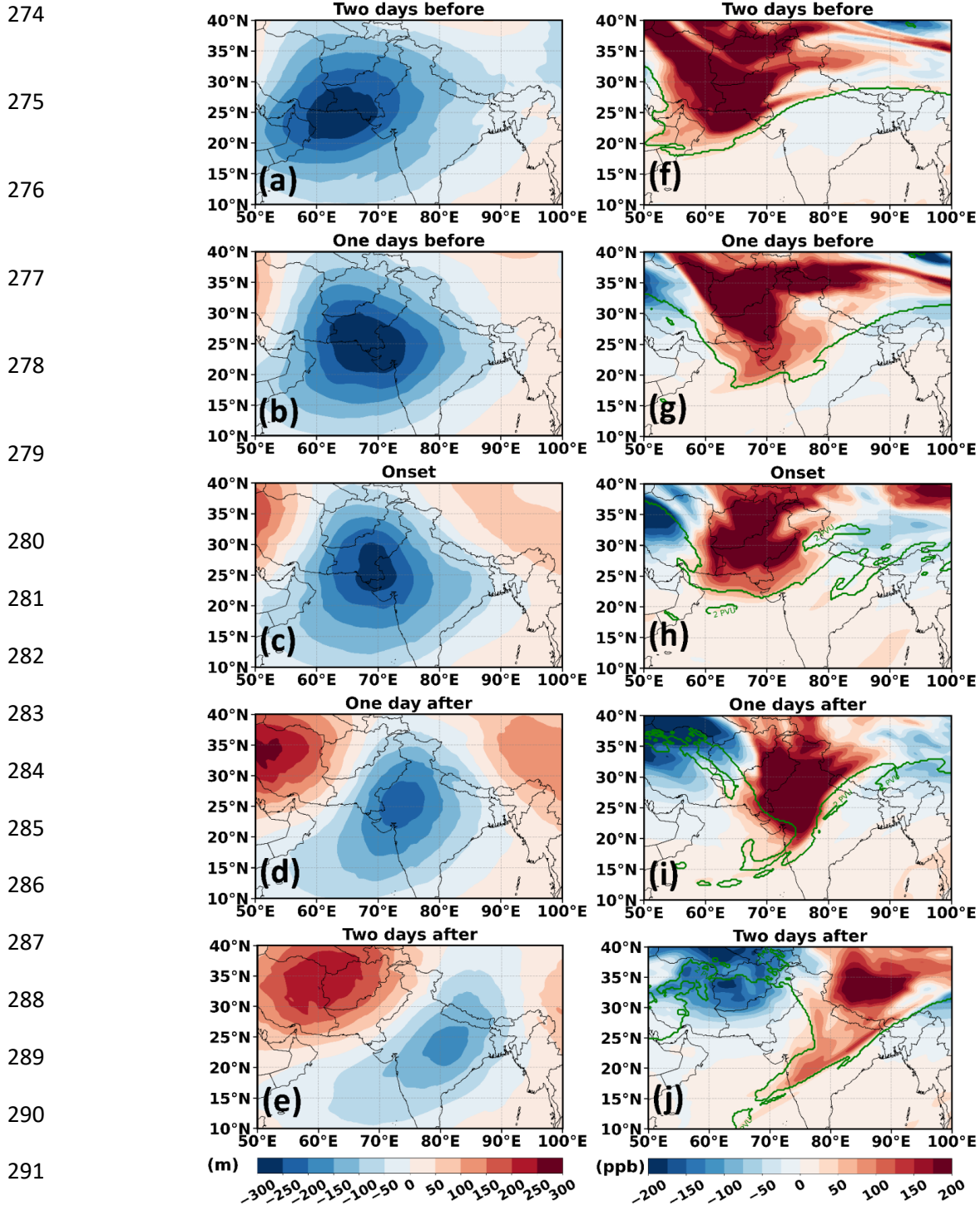
229 ~~In this section, we discuss the ozone enhancement in the UTLS over South Asia~~  
230 ~~associated with the 2018 SSW event and the possible mechanism responsible.~~ Figures 2a show  
231 vertical distribution of the temporal evolution of ozone anomalies averaged over South Asia for  
232 the 2018 SSW event. There is a large ozone enhancement in the UTLS, with values >80% (>150  
233 ppb) in 2018 within  $\pm 6$  days around the SSW-onset. Figure 2a indicates that the ozone  
234 enhancements in the UTLS region coincide with negative geopotential height (GPH) anomalies.  
235 Since the most pronounced ozone enhancement in the UTLS is observed within  $\pm 6$  days around  
236 the SSW onset, all subsequent analyses in this study are performed for this time period. The  
237 latitude–pressure (Fig. 2b) and longitude–pressure (Fig. 2c) cross-sections of ozone anomalies  
238 show large ozone enhancement for  $\pm 6$  days around the onset in the UTLS over South Asia,  
239 exceeding 60% (>80 ppb). Interestingly, a peak in ozone enhancement is seen at the subtropical  
240 jet core (Fig.2b). This suggests the role of the subtropical jet causing ozone enhancement in the  
241 upper troposphere over South Asia ~~(discussed in section 3.1.1)~~. The strong negative GPH  
242 anomaly (indicating a low-pressure area) coincident with large ozone enhancements, provides  
243 evidence of stratospheric intrusions occurring during the 2018 SSW event (Fig. 2c). **In addition,**  
244 **the reduced tropopause height near the onset in Fig.2a suggests the occurrence of tropopause**  
245  **folds. Earlier studies have shown that Rossby wave breaking (RWB) produces tropopause folds;**  
246  **provide an efficient pathway for quasi-isentropic descent of ozone-rich stratospheric air into the**  
247  **UTLS (Sprenger et al., 2003; Holtan et al., 1995).** Past literature reports ozone enhancements in  
248 the polar region associated with SSW (e.g., Baldwin et al., 2021); however, high ozone  
249 enhancement in the UTLS over the South Asian region underscores the unique regional impacts  
250 of SSWs.

### 251 ~~3.1.1 Causative Mechanisms for Changes in UTLS Ozone~~

252 ~~In this section~~ Further, we discuss the possible mechanism responsible for the ozone  
253 enhancement in the UTLS over South Asia associated with the 2018 SSW event. Several studies  
254 have shown that SSW-related planetary wave disturbances occur across a deep layer of the  
255 stratosphere (e.g., ~~McIntyre, 1982; McIntyre and Palmer, 1983;~~ Albers et al., 2016). These  
256 disturbances extend downward and disrupt horizontal flows in the upper troposphere (200 hPa)  
257 (Albers et al., 2016). To explore the influence of these disturbances over the South Asian region,  
258 we analysed GPH anomalies at 200 hPa. The evolution of GPH anomalies at 200 hPa for  $\pm 2$  days  
259 around the SSW onset (Feb. 12, 2018) is shown over the South Asian region in Fig. 3a-e and for  
260 the Northern Hemisphere in (Fig. S2a-e). In the Northern Hemisphere, patterns of high and low  
261 GPH anomalies at 200 hPa in the subtropical region (15-40°N) indicate the presence of synoptic-  
262 scale Rossby waves in the upper troposphere (Fig. S2a-e). The low GPH anomaly over South  
263 Asia (also see Fig. 3a-e) indicates a low-pressure area causing deepening of trough. It is  
264 associated with the eastward propagation of Rossby waves which can facilitate enhanced  
265 stratospheric intrusions.

266 RWB is characterised by large filaments of high-potential vorticity (PV) air extending  
267 towards the equator. The 2 PVU contour lines along with ozone anomaly maps at 200 hPa  
268 depicted in Fig. 3f-j shows clear indications of RWB causing ozone intrusions over South Asia.  
269 Such quasi-isentropic equatorward excursions cause irreversible ozone intrusion from the lower  
270 stratosphere into the upper troposphere (e.g., Holton et al., 1995; ~~Waugh and Polvani, 2000;~~  
271 ~~Albers et al., 2016~~).

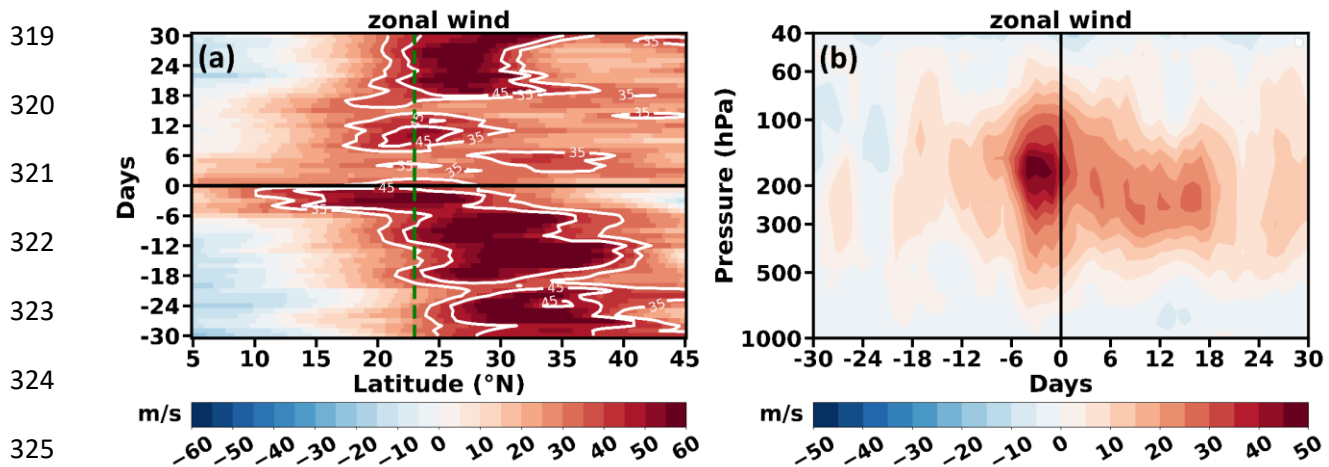
272  
273



292 **Figure 3.** Spatial map of (a-e) GPH anomaly at 200 hPa, (f-j) ozone anomaly at 200 hPa from 6  
 293 days before to 6 days after the onset of the 2018 SSW event, along with 2 PVU contour (green  
 294 solid line), shown at 3-day intervals. **The inside red square box represents the South-Asian region**  
 295 **considered for the present study. (Figure created using Python software).**

296            Figures 3f-j clearly show that intrusions near SSW onset days cause large ozone  
297    enhancements >150 ppb (>80%) over South Asia. Since the location and strength of the  
298    subtropical jet set the refractive waveguide and the location of wave breaking (Hoskins &  
299    Ambrizzi 1993; Hitchman & Huesmann 2007), we next diagnose the jet's evolution during this  
300    period. Figure 4 displays the latitude-time Hovmöller diagrams of zonal wind at 200 hPa and the  
301    time-altitude section around the onset over the South Asian region. Figure 4 clearly shows the  
302    equatorward shift of the subtropical jet around onset, creating the background flow conducive to  
303    the RWB and ozone intrusions seen in Fig. 3. The time evolution of zonal winds depicted in  
304    Figure 4a shows that thirty days before the onset, the subtropical jet core is positioned over the  
305    northern part of the Indian subcontinent, and migrates equatorward (south of 23°N) more  
306    prominently for ±6 days around the onset. The vertical variation of zonal wind (Fig. 4b) also  
307    indicates an equatorward displacement of the subtropical jet, with enhanced westerlies near 200  
308    hPa extending into 10–20°N over 65–90°E around the onset day. ~~clearly depicts the~~  
309    ~~intensification of westerly wind over the Indian region around 200 hPa close to the onset day,~~  
310    ~~facilitating Rossby wave breaking (Fig. 3b). The strength of zonal wind is strong within ±6 days~~  
311    ~~around the onset, causing higher ozone intrusions during this period (see Figs. 1b and 3b). Such~~  
312    changes in jet structure are consistent with a stronger upper-tropospheric Rossby-wave  
313    waveguide and background conditions under which RWB is more likely to occur near the  
314    tropopause (Hoskins and Ambrizzi 1993; Homeyer and Bowman 2013).

315  
316  
317  
318



319 **Figure 4.** (a) Latitude-time plot of zonal wind averaged over South Asia ( $65^{\circ} - 90^{\circ}$  E) at 200  
 320 hPa. (b) Temporal evolution of vertical zonal wind averaged over the South Asian region ( $65 -$   
 321  $90^{\circ}$  E,  $10 - 20^{\circ}$  N) for  $\pm 30$  days around the onset of the 2018 SSW event. The horizontal dashed  
 322 solid line in (a) and the vertical solid line in (b) represent the onset day. The vertical dashed line  
 323 in (a) represents  $23^{\circ}$ N. (Figure created using Python software).  
 324  
 325

326 The observed equatorward shift of the subtropical jet during the 2018 SSW may also be  
 327 influenced by the concurrent phase of the Quasi-Biennial Oscillation (QBO) (e.g., White et al.,  
 328 2016; Laehmy et al., 2014; Li et al., 2023). Notably, the February 2018 SSW took place during  
 329 the westerly phase of the QBO (Butler et al., 2020). Earlier studies have reported an equatorward  
 330 shift of the subtropical jet over the East Asia–North Pacific region during the westerly phase of  
 331 QBO (Park et al., 2021). Our analysis reveals a similar equatorward displacement of the  
 332 subtropical jet over South Asia during SSWs (Fig. 4a), coinciding with the westerly QBO phase.  
 333 During the westerly QBO, the associated secondary circulation warms the equatorial lower  
 334 stratosphere and cools the subtropics, sharpening and shifting the UTLS meridional temperature  
 335 gradient equatorward (e.g., Hitchman et al., 2021). By thermal-wind balance, this strengthens  
 336 upper-tropospheric westerlies on the equatorward flank and displaces the subtropical jet  
 337 equatorward over South Asian longitudes, favouring subtropical wave guidance, RWB, and PV-  
 338 streamer intrusions (Homeyer & Bowman, 2013; Albers et al., 2016). Additionally, previous  
 339 studies have shown that the westerly phase of QBO (WQBO) is associated with a lowering of the  
 340  
 341  
 342  
 343  
 344

345 tropopause (Collimore et al., 2003; Kumar et al., 2014). This lowering perturbs the subtropical  
346 waveguide structure and enhances tropopause fold activity (Kumar et al., 2020), thereby  
347 increasing the frequency of Rossby wave breaking and strengthening stratosphere–troposphere  
348 exchange, causing enhanced ozone intrusions.

### 349 **3.3 Composite UTLS Ozone Response during all SSW Events**

350 Further, we investigate the twenty-seven major SSW events from 1962 to 2017, to  
351 examine their influence on ozone variability in the upper troposphere over the South Asian  
352 region. ~~A detailed examination of individual SSW events revealed that ozone intrusions during  
353 some SSW events extend deeper and farther equatorward compared to others. Our analysis  
354 shows that, as in the 2018 case, SSW coinciding with the westerly phase of QBO (fifteen out of  
355 twenty-seven major SSW, WQBO-SSW) are associated with deeper and equatorward intrusion  
356 of ozone compared to those SSW coinciding with the Easterly phase of QBO (twelve out of  
357 twenty-seven, EQBO-SSW).~~ Motivated by the 2018 case study, we examined whether the QBO-  
358 phase dependence is evident across events. Table 1 lists all the major SSW events considered in  
359 this study along with their QBO phases. Of the 27 major SSWs, 15 occur during the westerly  
360 phase (WQBO-SSW) and 12 during the easterly phase (EQBO-SSW).

361 **Table 1.** List of all major SSW events from 1962 to 2018 considered for the present analysis  
362 alongside their onset dates and QBO phases at 70 hPa.

363

364

365

366

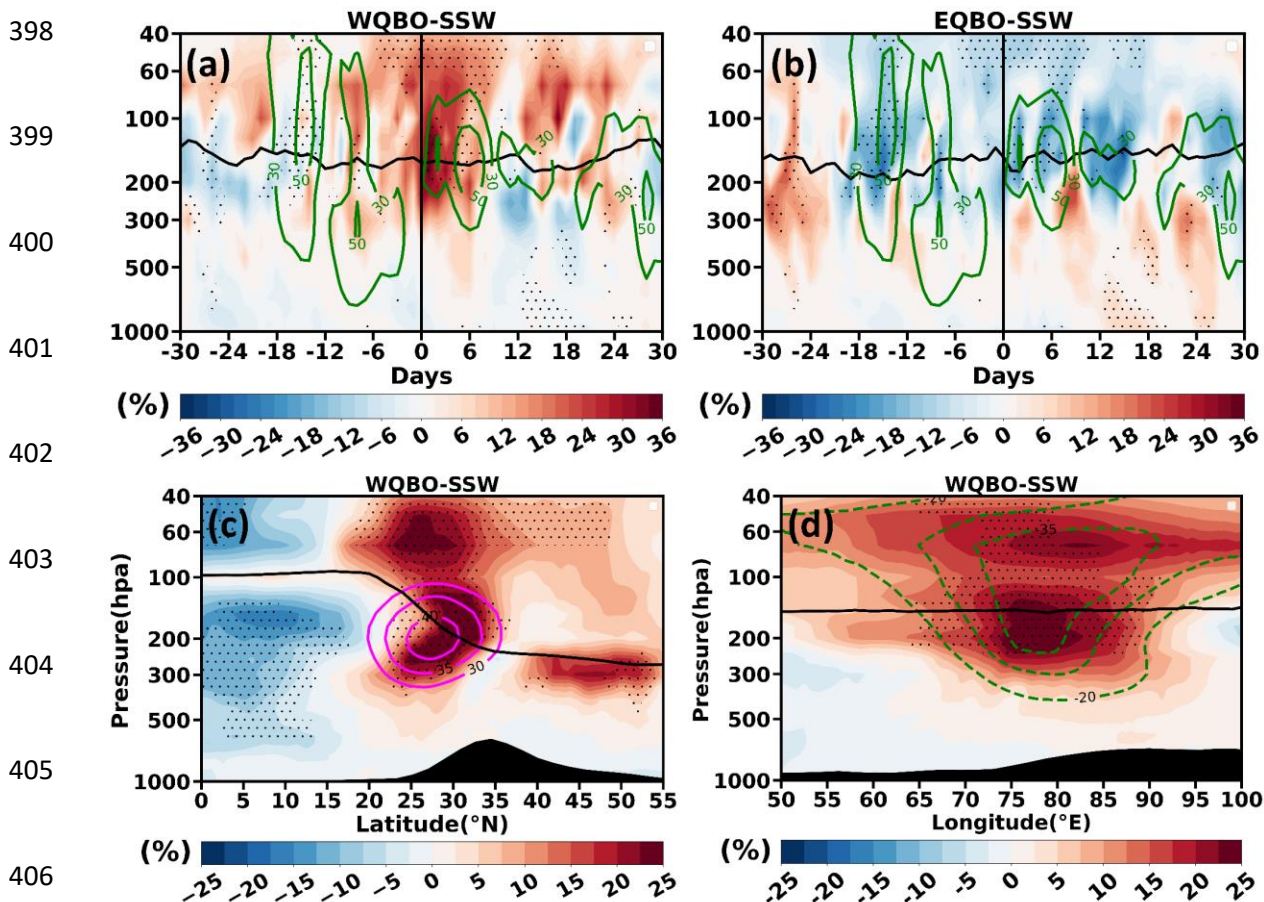
367

368  
369  
370  
371  
372  
373  
374  
375  
376  
377  
378  
379

<b>Year</b>	<b>Onset day</b>	<b>QBO Phase</b>
1963	28 January	Westerly
1966	23 February	Easterly
1968	7 January	Westerly
1969	13 March	Easterly
1970	2 January	Westerly
1971	18 January	Easterly
1973	31 January	Easterly
1977	9 January	Westerly
1979	22 February	Westerly
1980	29 February	Easterly
1981	4 March	Westerly
1984	24 February	Westerly
1985	1 January	Easterly
1987	23 January	Westerly
1988	14 March	Westerly
1989	21 February	Westerly
1999	26 February	Easterly
2000	20 March	Westerly
2001	11 February	Westerly
2003	18 January	Westerly
2004	5 January	Easterly
2006	21 January	Easterly
2007	24 February	Westerly
2008	22 February	Easterly
2009	24 January	Easterly
2010	9 February	Westerly
2013	6 January	Easterly
2018	12 February	Westerly

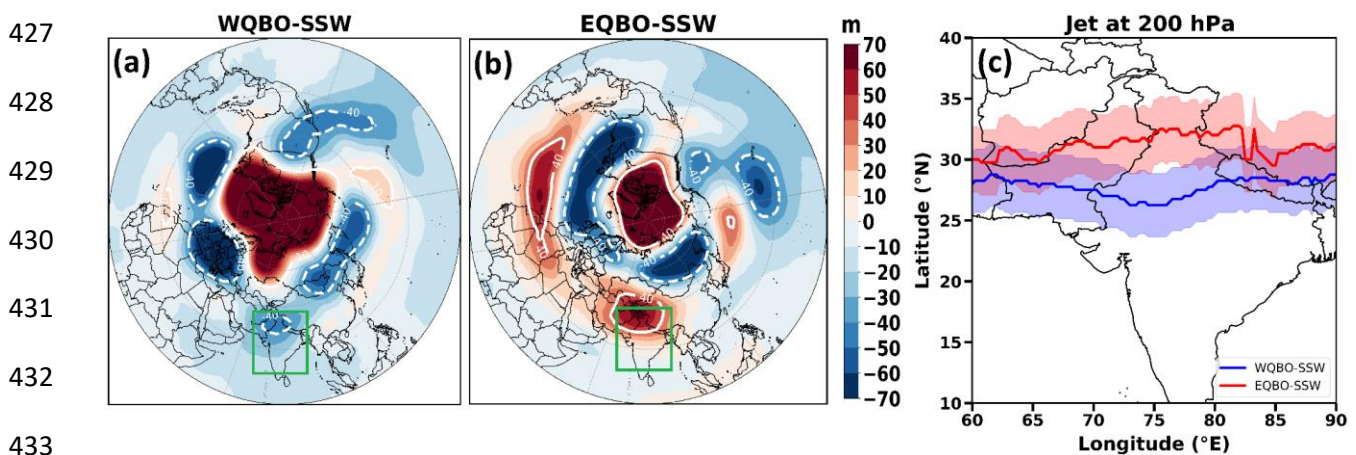
380 Previous studies have shown that the QBO phase can modulate the dynamical coupling  
381 between the stratosphere and troposphere during SSWs (Remya et al, 2023), influencing the  
382 extent of ozone transport into the upper troposphere (Zhang et al., 2021). Our analysis shows  
383 that, during the composite WQBO-SSW events, ozone intrudes down to 400 hPa, with anomalies  
384 exceeding ~30% (over 80 ppb) within  $\pm 6$  days of the onset (Fig. 5a). On the other hand, during  
385 the composite EQBO-SSW events, no significant ozone intrusion is evident within the same  
386 period (Fig. 5b). The latitude–pressure (Fig. 5c) and longitude–pressure (Fig. 5d) sections for  
387 WQBO-SSW further reveal enhanced ozone in the UTLS within  $\pm 6$  days over South Asia, with

388 anomalies exceeding 20% (>60 ppb). As seen earlier (Fig. 2b-c), the maximum ozone  
 389 enhancement in the WQBO-SSW composite is located near the subtropical jet core (Fig. 5c)  
 390 along with a strong negative GPH anomaly (Fig. 5d), indicating that jet dynamics and troughing  
 391 play a key role in modulating UTLS ozone responses during WQBO-SSW. ~~However, the~~  
 392 ~~amplitude of ozone enhancement in the UTLS is smaller in the composite of all WQBO-SSW than~~  
 393 ~~in 2018. This subdued effect is due to averaging across multiple episodic events occurring at~~  
 394 ~~different times within ±6 days around the SSW onset.~~ The enhancement in mean ozone of all  
 395 WQBO-SSW composite is smaller than in 2018, since there is variation in space and time of  
 396 ozone intrusions during individual SSW. The averaging across multiple events may subdue the  
 397 effect but it remains statistically significant over South Asia.



407 **Figure 5:** Temporal evolution of vertical ozone anomalies averaged over the South Asian region  
 408 (65-90°E, 20-35°N) from 30 days before to 30 days after the onset for (a) WQBO-SSW and (b)  
 409 EQBO-SSW. (c) Latitude-pressure cross-section of ozone anomalies averaged over South Asia  
 410 (65 - 90°E) for  $\pm 6$  days around all the WQBO-SSW onsets. (d) is the same as that of (c) but  
 411 represents the longitude variation of vertical ozone anomalies averaged over South Asia (20 -  
 412 35°N). The **horizontal solid line in (a-b) represents a 380 K potential temperature isoline, and the**  
 413 **vertical solid line in (a-b) represents the onset day.** Magenta contour lines in (c) represent the  
 414 mean zonal wind, and dashed green contour lines in (a,d) represent the negative GPH anomaly  
 415 and solid green contour lines in (b) represent the positive GPH anomaly. Solid black lines in (c-  
 416 d) represent the lapse rate tropopause. Black dots indicate a region of 95% confidence  
 417 level. **(Figure created using Python software).**

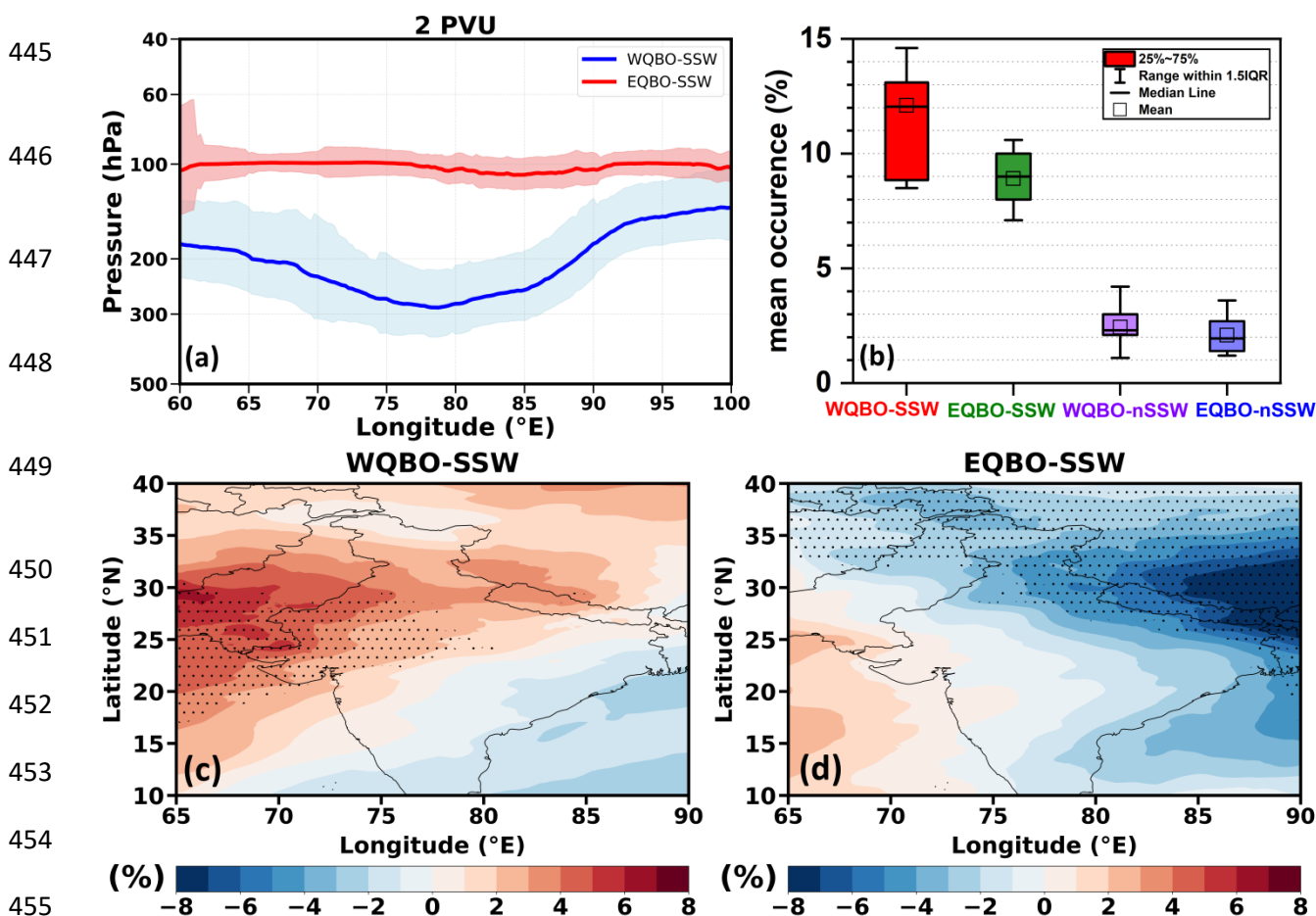
418 Further, we analysed the synoptic wave structure prevailing in the upper troposphere for  
 419 WQBO-SSW and EQBO-SSW composites within  $\pm 6$  days around the onset, using the 200 hPa  
 420 GPH anomaly as a proxy (Figs. 6a–b). The alternating trough–ridge patterns in GPH over the  
 421 subtropics indicate synoptic-scale Rossby waves in the upper troposphere. During the WQBO-  
 422 SSW a pronounced low GPH anomaly is observed over the South Asian region (Fig. 6a),  
 423 whereas high GPH dominates during the EQBO-SSW (Fig. 6b). The anomalous low over South  
 424 Asia during WQBO-SSW events indicates a deepening of the upper-tropospheric trough, which  
 425 favours the **tropopause folding and associated** stratospheric intrusions into the upper troposphere  
 426 (e.g., Knowland et al., 2017; Sprenger et al., 2007).



434 **Figure 6.** Spatial map of GPH anomaly for (a) WQBO-SSW and (b) EQBO-SSW and (c) jet  
 435 core at 200 hPa averaged for  $\pm 6$  days around the onset. White solid and dashed contour line in  
 436 (a-b) indicates positive and negative GPH anomaly. The square box in (a-b) represents the South

437 Asian region considered for the present study. Blue line and red line in (c) represents the jet core  
 438 for westerly phase and easterly phase of QBO respectively. The shading in (c) represents  
 439 standard error. (Figure created using Python software).

440 Further, we show the position of the subtropical jet core within  $\pm 6$  days around the SSW  
 441 onset for WQBO-SSW and EQBO-SSW. Figure 6c shows that during WQBO-SSW, the  
 442 subtropical jet shifts equatorward, with the jet core (blue lines) located south of  $30^\circ\text{N}$  over the  
 443 South Asian region. Whereas, during the EQBO-SSW, the jet core (red line) remains north of  
 444  $30^\circ\text{N}$ . (Detailed mechanism discussed in the section 3.2).



456 **Figure 7.** (a) Longitude-pressure cross section of 2PVU line averaged over South Asia (20-  
 457  $35^\circ\text{N}$ ) for WQBO-SSW and EQBO-SSW composites, shown for the days of maximum intrusion  
 458 selected within  $\pm 6$  days around the onset. The shading represents standard error. (b) Area-  
 459 averaged occurrence frequency (%) of Rossby wave breaking events during January-March over  
 460 South Asia identified from  $PV > 2$  and  $O_3 > 80$  ppbv at 300 hPa for WQBO-SSW, EQBO-  
 461 SSW, WQBO-nonSSW, and EQBO-nonSSW. (c) UTLS ozone anomaly composites (in %) for

462  $\pm 30$  days around onset for WQBO-SSW relative to WQBO-nonSSW. (d) same as that of (c) but  
463 for EQBO-SSW relative to EQBO-nonSSW. Stippling indicates a region of 95% confidence  
464 level. ~~(Figure created using Python software).~~

465 The PV-based RWB diagnostics for composite of WQBO-SSW and EQBO-SSW is  
466 shown in Figure 7a. For each event, the day of maximum intrusion within  $\pm 6$  days around the  
467 onset was chosen to capture the most representative feature, as averaging over the period tends to  
468 smooth out the signal. The longitude–pressure cross section (Fig. 7a) shows that during the  
469 WQBO-SSW, the 2 PVU contour extends farther downward into the upper troposphere,  
470 consistent with more pronounced tropopause folding and PV intrusion signatures ~~indicating~~  
471 ~~stronger PV intrusions~~. On the other hand, during EQBO-SSW events, the 2 PVU contour  
472 remains ~~confined to~~ at higher altitudes, suggesting weaker intrusions.

473 Further, we computed the occurrence frequency of RWB over South Asia during  
474 January–March for WQBO-SSW, EQBO-SSW, WQBO-nonSSW, and EQBO-nonSSW. Fig 7b  
475 shows the highest occurrence of  $\sim 12\%$  for WQBO-SSW, while RWB frequency is less for  
476 EQBO-SSW, WQBO-nonSSW, and EQBO-nonSSW. UTLS ozone also shows the highest  
477 enhancement for WQBO-SSW. Thus, equatorial shift of sub-tropical jet during WQBO-SSW  
478 causes RWB over south Asia leading to large ozone intrusions (Fig. 7d).

### 479 **3.4 Radiative Forcing of ozone associated with WQBO-SSWs over the South Asian region**

480 Further, we assessed instantaneous radiative forcing at the top of the atmosphere (TOA)  
481 due to ozone enhancements in (1) the UTLS and (2) total-column over the South Asian region  
482 associated with WQBO-SSW events. The instantaneous RF is computed for  $\pm 6$  days around the  
483 onset. RF at TOA due to the ozone enhancements in the UTLS is  $0.25 \pm 0.18 \text{ W.m}^{-2}$  for the 2018  
484 SSW, while the WQBO-SSW composite produces a forcing of  $0.09 \pm 0.05 \text{ W.m}^{-2}$ .

485 Further, the estimated RF at the TOA due to the total-column ozone changes is  $0.28 \pm$   
486  $0.19 \text{ W.m}^{-2}$  for the 2018 event and  $0.17 \pm 0.05 \text{ W.m}^{-2}$  for the composite. These results highlight  
487 the significant role of WQBO-SSW events in modulating the radiative balance ~~in the~~  
488 ~~troposphere, particularly in~~ at the UTLS TOA over South Asia. These changes in RF will affect  
489 UTLS temperature, stability, high clouds, and STE (e.g., Xia et al., 2018; Nowack et al., 2014).

#### 490 4. Conclusions

491 Using the ERA5 reanalysis (1962–2018), we investigated the impact of sudden  
492 stratospheric warmings (SSWs) on ozone variations in the UTLS (300–50 hPa) over South Asia.  
493 Unlike prior global analyses, we demonstrate that SSWs coinciding with the westerly phase of  
494 QBO (WQBO-SSW) lead to a substantial enhancement in UTLS ozone and radiative forcing  
495 over the South Asian region, whereas SSWs associated with the easterly phase of QBO (EQBO-  
496 SSW) do not. Our analysis shows that, unlike high latitudes, the South Asian response is not a  
497 direct downward influence. These low-latitude impacts are mediated by Rossby-wave dynamics.  
498 In particular, Rossby-wave breaking (RWB) and PV-streamer intrusions develop with the  
499 equatorward meandering of the subtropical jet.

500 We find that SSWs coinciding with the westerly phase of the QBO (WQBO-SSW) are  
501 associated with an equatorward shift (south of  $30^\circ\text{N}$  over South Asia) of the subtropical jet and  
502 lowering of tropopause which intensifies RWB and the largest UTLS ozone anomalies over  
503 South Asia. An enhancement in ozone anomalies (ranging from 30 to 80% or 80 to 150 ppb for  
504 composite and 2018) in the UTLS is noted during the WQBO-SSW years relative to the non-  
505 SSW calendar-day climatology within  $\pm 6$  days of onset. This ozone enhancement in the UTLS  
506 during WQBO-SSW events contributes an instantaneous radiative forcing at the top of the  
507 atmosphere of  $0.25 \pm 0.18 \text{ W.m}^{-2}$  for the 2018 and  $0.09 \pm 0.05 \text{ W.m}^{-2}$  during the composite. Due

508 to total-column ozone changes, instantaneous RF at the top of the atmosphere increases by 0.28  
509  $\pm 0.19 \text{ W.m}^{-2}$  for 2018 and  $0.17 \pm 0.05 \text{ W.m}^{-2}$  for the WQBO-SSW composite. This positive  
510 TOA radiative forcing does not necessarily imply surface warming, as ozone perturbations can  
511 also induce negative surface radiative forcing. For example, Williams et al. (2024) reported a  
512 surface forcing of  $-0.36 \text{ W.m}^{-2}$  associated with ozone changes in the UTLS. Our radiative kernel  
513 method does not estimate a surface forcing associated with ozone changes in the UTLS. The  
514 enhancement in ozone and associated RF can affect the stability and temperature of the UTLS,  
515 high clouds, and STE. However, such analysis is beyond the scope of the present study.

516 ~~This large increase in radiative forcing produces positive feedback on the warming~~  
517 ~~climate of this region. Ozone intrusions are warranted to elevate pollution effects and climate~~  
518 ~~warming, impacting people's health, the ecosystem, and the economy. In addition, the frequency~~  
519 ~~of SSW is projected to increase in a warming climate (Kim et al., 2017), which will further~~  
520 ~~increase stratospheric ozone intrusions and potentially amplify the consequences of positive~~  
521 ~~feedback mechanisms.~~ Since the evolution of the polar vortex modulates subtropical Rossby-  
522 wave guides that affect South Asia, these stratospheric influences must be represented in regional  
523 prediction systems. ~~We emphasise that climate models should be extended to the stratosphere,~~  
524 ~~including polar vortex dynamics, for accurate prediction of climate over South Asia.~~ Earlier  
525 studies have shown that using high-top, stratosphere-resolving models improve subseasonal-to-  
526 seasonal predictability (Hardiman et al., 2012; Charlton-Perez et al., 2013; Scaife et al., 2022).  
527 We emphasise that models should be extended to the stratosphere, including polar vortex  
528 dynamics, for accurate sub seasonal-to-seasonal prediction over South Asia.

529  
530

531  
532  
533  
534  
535  
536  
537  
538  
539  
540  
541  
542  
543  
544  
545  
546  
547  
548  
549  
550  
551  
552

### **Code and data availability**

The ERA5 data that support the findings of this study are openly available from <https://cds.climate.copernicus.eu/> (10.24381/cds.bd0915c6). All the Figures are created using the Python software. The python code used to plot figures in this paper are available from <https://doi.org/10.5281/zenodo.17639489>

### **Acknowledgements**

The authors thank the staff of the High Power Computing Centre (HPC) in IITM, Pune, India, for providing computer resources and the team members of ERA5 for providing data. The authors are thankful to three anonymous reviewers for their valuable suggestions.

### **Author contributions**

Conceptualisation: S.F. Supervision: SF, MH, RF Investigation and methodology: SC, SR, VS, and PC. Writing: all authors.

### **Competing interests**

At least one of the (co-)authors is a member of the editorial board of Atmospheric Chemistry and Physics.

553 **References:**

- 554 Albers, J. R., Kiladis, G. N., Birner, T. and Dias, J.: Tropical upper-tropospheric potential  
555 vorticity intrusions during sudden stratospheric warmings, *Journal of the Atmospheric*  
556 *Sciences*, 73(6), 2361–2384, doi:10.1175/jas-d-15-0238.1, 2016.
- 557 Baldwin, M. P. and Dunkerton, T. J.: Stratospheric harbingers of anomalous weather regimes,  
558 *Science*, 294(5542), 581–584, doi:10.1126/science.1063315, 2001.
- 559 Baldwin, M. P., Domeisen, D. I. V., Hegglin, M. I., Garny, H., Garfinkel, C. I., Langematz, U.,  
560 Charlton-Perez, A. J., Butchart, N., Gerber, E. P., Birner, T., Butler, A. H., Ayarzagüena, B.,  
561 and Pedatella, N. M.: Sudden Stratospheric Warmings, *Reviews of Geophysics*, 59,  
562 <https://doi.org/10.1029/2020rg000708>, 2021.
- 563 Butler, A. H., Seidel, D. J., Hardiman, S. C., Butchart, N., Birner, T. and Match, A.: Defining  
564 sudden stratospheric warmings, *Bulletin of the American Meteorological Society*, 96(11),  
565 1913–1928, doi:10.1175/bams-d-13-00173.1, 2015.
- 566 Butler, A. H., Lillo, S. P., Long, C. S., Lee, S. H., and Lawrence, Z. D.: Differences between the  
567 2018 and 2019 stratospheric polar vortex split events, *Quarterly Journal of the Royal*  
568 *Meteorological Society*, 146, 3503–3521, <https://doi.org/10.1002/qj.3858>, 2020.
- 569 Charlton, A. J. and Polvani, L. M.: A new look at stratospheric sudden warmings. part I:  
570 Climatology and modeling benchmarks, *Journal of Climate*, 20(3), 449–469,  
571 doi:10.1175/jcli3996.1, 2007.
- 572 Charlton-Perez, A. J., Polvani, L. M., Austin, J. and Li, F.: The frequency and dynamics of  
573 stratospheric sudden warmings in the 21st century, *Journal of Geophysical Research:*  
574 *Atmospheres*, 113(D16), doi:10.1029/2007jd009571, 2008.
- 575 Charlton-Perez, A. J., Baldwin, M. P., Shaw, T. A., Hardiman, S., Polvani, L., Shindell, D.,  
576 Yoden, S., Gerber, E. P., Manzini, E., Calvo, N., Yukimoto, S., Lott, F., Davis, N. A., Black,  
577 R. X., Butler, A. H., Krüger, K., Son, S., Kim, J., Lee, Y., Mcdaniel, B. A., Reichler, T.,  
578 Christiansen, B., Watanabe, S., Toohey, M., Sigmond, M., Gillett, N., Wilcox, L., and  
579 Birner, T.: On the lack of stratospheric dynamical variability in low-top versions of the  
580 CMIP5 models, *Journal of Geophysical Research: Atmospheres*, 118, 2494–2505,  
581 <https://doi.org/10.1002/jgrd.50125>, 2013.
- 582 Collimore, C. C., Huesmann, A., Martin, D. W., Hitchman, M. H., and Waliser, D. E.: On The  
583 Relationship between the QBO and Tropical Deep Convection, *Journal of Climate*, 16,  
584 2552–2568, [https://doi.org/10.1175/1520-0442\(2003\)016<2552:otrbtq>2.0.co;2](https://doi.org/10.1175/1520-0442(2003)016<2552:otrbtq>2.0.co;2), 2003.

585 Dewan, S. and Lakhani, A.: Tropospheric ozone and its natural precursors impacted by climatic  
586 changes in emission and dynamics, *Frontiers in Environmental Science*, 10,  
587 doi:10.3389/fenvs.2022.1007942, 2022.

588 Domeisen, D. I. and Butler, A. H.: Stratospheric drivers of extreme events at the Earth's surface,  
589 *Communications Earth & Environment*, 1(1), doi:10.1038/s43247-020-00060-z, 2020.

590 Domeisen, D. I., Grams, C. M. and Papritz, L.: The role of North Atlantic–European weather  
591 regimes in the surface impact of sudden stratospheric warming events, *Weather and Climate  
592 Dynamics*, 1(2), 373–388, doi:10.5194/wcd-1-373-2020, 2020.

593 Fadnavis, S., Chakraborty, T., and Beig, G.: Seasonal stratospheric intrusion of ozone in the  
594 upper troposphere over India, *Annales Geophysicae*, 28, 2149–2159,  
595 <https://doi.org/10.5194/angeo-28-2149-2010>, 2010.

596 Fadnavis, S., Wienhold, F. G., Müller, R., Oelsner, P., Vogel, B., Naja, M., Sonbawne, S.,  
597 Dirksen, R., Sagalgile, A., and Peter, T.: Comparison of ozonesonde measurements in the  
598 upper troposphere and lower Stratosphere in Northern India with reanalysis and chemistry-  
599 climate-model data, *Scientific Reports*, 13, <https://doi.org/10.1038/s41598-023-34330-5>,  
600 2023.

601 Feng, Z., Agathokleous, E., Yue, X., Oksanen, E., Paoletti, E., Sase, H., Gandin, A., Koike, T.,  
602 Calatayud, V., Yuan, X., Liu, X., De Marco, A., Jolivet, Y., Kontunen-Soppela, S., Hoshika,  
603 Y., Saji, H., Li, P., Li, Z., Watanabe, M. and Kobayashi, K.: Emerging challenges of ozone  
604 impacts on Asian plants: Actions are needed to protect ecosystem health, *Ecosystem Health  
605 and Sustainability*, 7(1), doi:10.1080/20964129.2021.1911602, 2021.

606 Fleming, Z. L., Doherty, R. M., von Schneidmesser, E., Malley, C. S., Cooper, O. R., Pinto, J.  
607 P., Colette, A., Xu, X., Simpson, D., Schultz, M. G., Lefohn, A. S., Hamad, S., Moolla, R.,  
608 Solberg, S. and Feng, Z.: Tropospheric Ozone Assessment Report: Present-day ozone  
609 distribution and trends relevant to human health, *Elementa: Science of the Anthropocene*, 6,  
610 doi:10.1525/elementa.273, 2018.

611 Hall, R. J., Mitchell, D. M., Seviour, W. J. and Wright, C. J.: Tracking the stratosphere-to-  
612 surface impact of sudden stratospheric warmings, *Journal of Geophysical Research:  
613 Atmospheres*, 126(3), doi:10.1029/2020jd033881, 2021.

614 Hardiman, S. C., Butchart, N., Hinton, T. J., Gray, L. J., and Osprey, S. M.: The Effect of a  
615 Well-Resolved Stratosphere on Surface Climate: Differences between CMIP5 Simulations  
616 with High and Low Top Versions of the Met Office Climate Model, *Journal of Climate*, 25,  
617 7083–7099, <https://doi.org/10.1175/jcli-d-11-00579.1>, 2012.

618 Hersbach, H., Bell, B., Berrisford, P., Hirahara, S., Horányi, A., Muñoz-Sabater, J., Nicolas, J.,  
619 Peubey, C., Radu, R., Schepers, D., Simmons, A., Soci, C., Abdalla, S., Abellan, X.,  
620 Balsamo, G., Bechtold, P., Biavati, G., Bidlot, J., Bonavita, M., De Chiara, G., Dahlgren, P.,  
621 Dee, D., Diamantakis, M., Dragani, R., Flemming, J., Forbes, R., Fuentes, M., Geer, A.,  
622 Haimberger, L., Healy, S., Hogan, R. J., Hólm, E., Janisková, M., Keeley, S., Laloyaux, P.,  
623 Lopez, P., Lupu, C., Radnoti, G., de Rosnay, P., Rozum, I., Vamborg, F., Villaume, S. and  
624 Thépaut, J.: The ERA5 global reanalysis, *Quarterly Journal of the Royal Meteorological*  
625 *Society*, 146(730), 1999–2049, doi:10.1002/qj.3803, 2020.

626 Hitchman, M. H. and Huesmann, A. S.: A Seasonal Climatology of Rossby Wave Breaking in  
627 the 320–2000-K Layer, *Journal of the Atmospheric Sciences*, 64, 1922–1940,  
628 <https://doi.org/10.1175/jas3927.1>, 2007.

629 Hitchman, M. H., Tegtmeier, S., Yoden, S., Haynes, P. H., and Kumar, V.: An Observational  
630 History of the Direct Influence of the Stratospheric Quasi-biennial Oscillation on the  
631 Tropical and Subtropical Upper Troposphere and Lower Stratosphere, *Journal of the*  
632 *Meteorological Society of Japan. Ser. II*, 99, 239–267, [https://doi.org/10.2151/jmsj.2021-](https://doi.org/10.2151/jmsj.2021-012)  
633 012, 2021.

634 Hoffmann, L. and Spang, R.: An assessment of tropopause characteristics of the ERA5 and era-  
635 interim meteorological reanalyses, *Atmospheric Chemistry and Physics*, 22(6), 4019–4046,  
636 doi:10.5194/acp-22-4019-2022, 2022.

637 Holton, J. R., Haynes, P. H., McIntyre, M. E., Douglass, A. R., Rood, R. B. and Pfister, L.:  
638 Stratosphere-Troposphere exchange, *Reviews of Geophysics*, 33(4), 403–439,  
639 doi:10.1029/95rg02097, 1995.

640 Homeyer, C. R. and Bowman, K. P.: Rossby Wave Breaking and Transport between the Tropics  
641 and Extratropics above the Subtropical Jet, *Journal of the Atmospheric Sciences*, 70, 607–  
642 626, <https://doi.org/10.1175/jas-d-12-0198.1>, 2013.

643 Hoskins, B. J. and Ambrizzi, T.: Rossby Wave Propagation on a Realistic Longitudinally  
644 Varying Flow, *Journal of the Atmospheric Sciences*, 50, 1661–1671,  
645 [https://doi.org/10.1175/1520-0469\(1993\)050<1661:rwpoar>2.0.co;2](https://doi.org/10.1175/1520-0469(1993)050<1661:rwpoar>2.0.co;2), 1993.

646 Iglesias-Suarez, F., Kinnison, D. E., Rap, A., Maycock, A. C., Wild, O. and Young, P. J.: Key  
647 drivers of ozone change and its radiative forcing over the 21st century, *Atmospheric*  
648 *Chemistry and Physics*, 18(9), 6121–6139, doi:10.5194/acp-18-6121-2018, 2018.

649 Kidston, J., Scaife, A. A., Hardiman, S. C., Mitchell, D. M., Butchart, N., Baldwin, M. P. and  
650 Gray, L. J.: Stratospheric influence on tropospheric jet streams, storm tracks and Surface  
651 Weather, *Nature Geoscience*, 8(6), 433–440, doi:10.1038/ngeo2424, 2015.

652 Kim, J., Park, H.-S., Son, S.-W., and Gerber, E. P.: Defining Sudden Stratospheric Warming in  
653 Climate Models: Accounting for Biases in Model Climatologies, *Journal of Climate*, 30,  
654 5529–5546, <https://doi.org/10.1175/jcli-d-16-0465.1>, 2017.

655 Knowland, K. E., Ott, L. E., Duncan, B. N. and Wargan, K.: Stratospheric intrusion-influenced  
656 ozone air quality exceedances investigated in the NASA Merra-2 Reanalysis, *Geophysical  
657 Research Letters*, 44(20), doi:10.1002/2017gl074532, 2017.

658 Kumar, V., Dhaka, S. K., Reddy, K. K., Gupta, A., Prasad, S. B. S., Panwar, V., Singh, N., Ho,  
659 S.-P., and Takahashi, M.: Impact of quasi-biennial oscillation on the inter-annual variability  
660 of the tropopause height and temperature in the tropics: A study using  
661 COSMIC/FORMOSAT-3 observations, *Atmospheric Research*, 139, 62–70,  
662 <https://doi.org/10.1016/j.atmosres.2013.12.014>, 2014.

663 Kumar, K. N., Sharma, S. K., Naja, M., and Phanikumar, D. V.: A Rossby wave breaking-  
664 induced enhancement in the tropospheric ozone over the Central Himalayan region,  
665 *Atmospheric Environment*, 224, 117356, <https://doi.org/10.1016/j.atmosenv.2020.117356>,  
666 2020.

667 Kunz, A., Konopka, P., Müller, R. and Pan, L. L.: Dynamical tropopause based on isentropic  
668 potential vorticity gradients, *Journal of Geophysical Research*, 116(D1),  
669 doi:10.1029/2010jd014343, 2011.

670 Lee, J., Butler, A. H., Albers, J. R., Wu, Y. and Lee, S. H.: Impact of sudden stratospheric  
671 warmings on the stratosphere-to-troposphere transport of ozone, *Geophysical Research  
672 Letters*, 52(2), doi:10.1029/2024gl112588, 2025.

673 Li, H., Fan, Y., Li, Q., Ji, X., Zhang, J., and Sheng, B.: The Gravity Wave Activity during Two  
674 Recent QBO Disruptions Revealed by U.S. High-Resolution Radiosonde Data, *Remote  
675 Sensing*, 15, 472, <https://doi.org/10.3390/rs15020472>, 2023.

676 Li, Y., Xia, Y., Xie, F. and Yan, Y.: Influence of stratosphere-troposphere exchange on long-  
677 term trends of surface ozone in CMIP6, *Atmospheric Research*, 297, 107086,  
678 doi:10.1016/j.atmosres.2023.107086, 2024.

679 Lim, S. S., Vos, T., Flaxman, A. D., Danaei, G., Shibuya, K., Adair-Rohani, H., AlMazroa, M.  
680 A., Amann, M., Anderson, H. R., Andrews, K. G., Aryee, M., Atkinson, C., Bacchus, L. J.,  
681 Bahalim, A. N., Balakrishnan, K., Balmes, J., Barker-Collo, S., Baxter, A., Bell, M. L.,  
682 Blore, J. D., Blyth, F., Bonner, C., Borges, G., Bourne, R., Boussinesq, M., Brauer, M.,  
683 Brooks, P., Bruce, N. G., Brunekreef, B., Bryan-Hancock, C., Bucello, C., Buchbinder, R.,  
684 Bull, F., Burnett, R. T., Byers, T. E., Calabria, B., Carapetis, J., Carnahan, E., Chafe, Z.,  
685 Charlson, F., Chen, H., Chen, J. S., Cheng, A. T.-A., Child, J. C., Cohen, A., Colson, K. E.,

686 Cowie, B. C., Darby, S., Darling, S., Davis, A., Degenhardt, L., Dentener, F., Des Jarlais, D.  
687 C., Devries, K., Dherani, M., Ding, E. L., Dorsey, E. R., Driscoll, T., Edmond, K., Ali, S. E.,  
688 Engell, R. E., Erwin, P. J., Fahimi, S., Falder, G., Farzadfar, F., Ferrari, A., Finucane, M. M.,  
689 Flaxman, S., Fowkes, F. G., Freedman, G., Freeman, M. K., Gakidou, E., Ghosh, S.,  
690 Giovannucci, E., Gmel, G., Graham, K., Grainger, R., Grant, B., Gunnell, D., Gutierrez, H.  
691 R., Hall, W., Hoek, H. W., Hogan, A., Hosgood, H. D., Hoy, D., Hu, H., Hubbell, B. J.,  
692 Hutchings, S. J., Ibeanusi, S. E., Jacklyn, G. L., Jasrasaria, R., Jonas, J. B., Kan, H., Kanis, J.  
693 A., Kassebaum, N., Kawakami, N., Khang, Y.-H., Khatibzadeh, S., Khoo, J.-P., et al.: A  
694 comparative risk assessment of burden of disease and injury attributable to 67 risk factors  
695 and risk factor clusters in 21 regions, 1990–2010: A systematic analysis for the global  
696 burden of disease study 2010, *The Lancet*, 380(9859), 2224–2260, doi:10.1016/s0140-  
697 6736(12)61766-8, 2012.

698 Lin, Y., Jiang, F., Zhao, J., Zhu, G., He, X., Ma, X., Li, S., Sabel, C. E. and Wang, H.: Impacts  
699 of O<sub>3</sub> on premature mortality and crop yield loss across China, *Atmospheric Environment*,  
700 194, 41–47, doi:10.1016/j.atmosenv.2018.09.024, 2018.

701 Liu, Y., Gao, S. T., Brasseur, G., Tie, X. X., Wang, H. P., Kinnison, D., and Liu, C. X.:  
702 Atmospheric tracers during the 2003–2004 stratospheric warming event and impact of ozone  
703 intrusions in the troposphere, *Atmospheric Chemistry and Physics*, 9, 2157–2170,  
704 <https://doi.org/10.5194/acp-9-2157-2009>, 2009.

705 Ma, X., Huang, J., Hegglin, M., Joeckel, P. and Zhao, T.: Causes of growing middle-upper  
706 tropospheric ozone over the Northwest Pacific Region, doi:10.5194/egusphere-2023-2411,  
707 2024.

708 Myhre, G., & Stordal, F.: Role of spatial and temporal variations in the computation of radiative  
709 forcing and GWP. *Journal of Geophysical Research: Atmospheres*, 102(D10), 11181–11200.  
710 <https://doi.org/10.1029/97jd00148>, 1997.

711 Myhre, G., Shine, K. P., Rädcl, G., Gauss, M., Isaksen, I. S. A., Tang, Q., Prather, M. J.,  
712 Williams, J. E., van Velthoven, P., Dessens, O., Koffi, B., Szopa, S., Hoor, P., Grewe, V.,  
713 Borken-Kleefeld, J., Berntsen, T. K. and Fuglestedt, J. S.: Radiative forcing due to changes  
714 in ozone and methane caused by the transport sector, *Atmospheric Environment*, 45(2), 387–  
715 394, doi:10.1016/j.atmosenv.2010.10.001, 2011.

716 Nowack, P. J., Luke Abraham, N., Maycock, A. C., Braesicke, P., Gregory, J. M., Joshi, M. M.,  
717 Osprey, A. and Pyle, J. A.: A large ozone-circulation feedback and its implications for  
718 global warming assessments, *Nature Climate Change*, 5(1), 41–45,  
719 doi:10.1038/nclimate2451, 2014.

- 720 Park, C., Choi, J., Son, S., and Lim, Y.: Quasi-biennial oscillation-related surface air temperature  
721 change over the western North Pacific in late winter, *International Journal of Climatology*,  
722 42, 4351–4359, <https://doi.org/10.1002/joc.7470>, 2021.
- 723 Remya, R., Manoj, M. G., and Mohanakumar, K.: Role of Quasi-Biennial oscillation on the link  
724 between sudden stratospheric warming and tropical weather events, *Advances in Space*  
725 *Research*, 73, 571–584, <https://doi.org/10.1016/j.asr.2023.11.006>, 2023.
- 726 Roy, C., Thazhe Purayil, S., and Fadnavis, S.: The stratospheric ozone rich cold intrusion during  
727 El-Nino over the Indian region: implication during the Indian summer monsoon,  
728 <https://doi.org/10.5194/egusphere-egu2020-937>, 2020.
- 729 Roy, C., Ravishankara, A. R., Newman, P. A., David, L. M., Fadnavis, S., Rathod, S. D., Lait,  
730 L., Krishnan, R., Clark, H. and Sauvage, B.: Estimation of stratospheric intrusions during  
731 Indian Cyclones, *Journal of Geophysical Research: Atmospheres*, 128(3),  
732 [doi:10.1029/2022jd037519](https://doi.org/10.1029/2022jd037519), 2023.
- 733 Scaife, A. A., Charlton-Perez, A. J., Son, S.-W., Hardiman, S. C., Polvani, L., Lim, E.-P.,  
734 Haynes, P., Baldwin, M. P., Shepherd, T. G., Perlwitz, J., Richter, J. H., Noguchi, S.,  
735 Thompson, D. W. J., Karpechko, A. Y., Butler, A. H., Scinocca, J., Sigmond, M., Domeisen,  
736 D. Shi. V., and Garfinkel, C. I.: Long-range prediction and the stratosphere, *Atmospheric*  
737 *Chemistry and Physics*, 22, 2601–2623, <https://doi.org/10.5194/acp-22-2601-2022>, 2022.
- 738 Schimanke, S., Spanghel, T., Huebener, H. and Cubasch, U.: Variability and trends of major  
739 stratospheric warmings in simulations under constant and increasing GHG concentrations,  
740 *Climate Dynamics*, 40(7–8), 1733–1747, [doi:10.1007/s00382-012-1530-x](https://doi.org/10.1007/s00382-012-1530-x), 2012.
- 741 Shell, K. M., Kiehl, J. T. and Shields, C. A.: Using the radiative kernel technique to calculate  
742 climate feedbacks in NCAR’s community atmospheric model, *Journal of Climate*, 21(10),  
743 2269–2282, [doi:10.1175/2007jcli2044.1](https://doi.org/10.1175/2007jcli2044.1), 2008.
- 744 Shi, Y., Evtushevsky, O., Milinevsky, G., Wang, X., Klekociuk, A., Han, W., Grytsai, A., Wang,  
745 Y., Wang, L., Novosyadlyj, B., and Andrienko, Y.: Impact of the 2018 major sudden  
746 stratospheric warming on weather over the midlatitude regions of Eastern Europe and East  
747 Asia, *Atmospheric Research*, 297, 107112, <https://doi.org/10.1016/j.atmosres.2023.107112>,  
748 2023.
- 749 Sigmond, M., Scinocca, J. F., Kharin, V. V. and Shepherd, T. G.: Enhanced seasonal forecast  
750 skill following stratospheric sudden warmings, *Nature Geoscience*, 6(2), 98–102,  
751 [doi:10.1038/ngeo1698](https://doi.org/10.1038/ngeo1698), 2013.
- 752 Skeie, R. B., Myhre, G., Hodnebrog, Ø., Cameron-Smith, P. J., Deushi, M., Hegglin, M. I.,  
753 Horowitz, L. W., Kramer, R. J., Michou, M., Mills, M. J., Olivie, D. J., Connor, F. M.,

754 Paynter, D., Samset, B. H., Sellar, A., Shindell, D., Takemura, T., Tilmes, S. and Wu, T.:  
755 Historical total ozone radiative forcing derived from CMIP6 simulations, *npj Climate and*  
756 *Atmospheric Science*, 3(1), doi:10.1038/s41612-020-00131-0, 2020.

757 SPARC Reanalysis Intercomparison Project (S-RIP) Final Report. M. Fujiwara, G.L. Manney,  
758 L.J. Gray, and J.S. Wright (Eds.), SPARC Report No. 10, WCRP-17/2020, doi:  
759 10.17874/800dee57d13, available at [www.sparc-climate.org/publications/sparc-reports](http://www.sparc-climate.org/publications/sparc-reports),  
760 2022.

761 Sprenger, M., Croci Maspoli, M. and Wernli, H.: Tropopause folds and cross-Tropopause  
762 Exchange: A global investigation based upon ECMWF analyses for the time period March  
763 2000 to February 2001, *Journal of Geophysical Research: Atmospheres*, 108(D12),  
764 doi:10.1029/2002jd002587, 2003.

765 Sprenger, M., Wernli, H. and Bourqui, M.: Stratosphere–troposphere exchange and its relation to  
766 potential vorticity streamers and cutoffs near the extratropical tropopause, *Journal of the*  
767 *Atmospheric Sciences*, 64(5), 1587–1602, doi:10.1175/jas3911.1, 2007.

768 Stamnes, K., Tsay, S.-C., Wiscombe, W. and Jayaweera, K.: Numerically stable algorithm for  
769 discrete-ordinate-method radiative transfer in multiple scattering and emitting layered  
770 media, *Applied Optics*, 27(12), 2502, doi:10.1364/ao.27.002502, 1988.

771 Wang, H., Lu, X., Jacob, D. J., Cooper, O. R., Chang, K.-L., Li, K., Gao, M., Liu, Y., Sheng, B.,  
772 Wu, K., Wu, T., Zhang, J., Sauvage, B., Nédélec, P., Blot, R. and Fan, S.: Global  
773 tropospheric ozone trends, attributions, and radiative impacts in 1995–2017: An integrated  
774 analysis using aircraft (IAGOS) observations, ozonesonde, and multi-decadal chemical  
775 model simulations, *Atmospheric Chemistry and Physics*, 22(20), 13753–13782,  
776 doi:10.5194/acp-22-13753-2022, 2022.

777 Wang, M. and Fu, Q.: Stratosphere-troposphere exchange of Air Masses and ozone  
778 concentrations based on reanalyses and observations, *Journal of Geophysical Research:*  
779 *Atmospheres*, 126(18), doi:10.1029/2021jd035159, 2021.

780 Waugh, D. W. and Polvani, L. M.: Climatology of intrusions into the tropical upper troposphere,  
781 *Geophysical Research Letters*, 27(23), 3857–3860, doi:10.1029/2000gl012250, 2000.

782 White, I. P., Lu, H., and Mitchell, N. J.: Seasonal evolution of the QBO-induced wave forcing  
783 and circulation anomalies in the northern winter stratosphere, *Journal of Geophysical*  
784 *Research: Atmospheres*, 121, 10,411-10,431, <https://doi.org/10.1002/2015jd024507>, 2016.

785 Williams, R. S., Hegglin, M. I., Jöckel, P., Garny, H. and Shine, K. P.: Air quality and radiative  
786 impacts of downward-propagating sudden stratospheric warmings (ssws), *Atmospheric*  
787 *Chemistry and Physics*, 24(2), 1389–1413, doi:10.5194/acp-24-1389-2024, 2024.

788 Williams, R. S., Hegglin, M. I., Kerridge, B. J., Jöckel, P., Latter, B. G., and Plummer, D. A.:  
789 Characterising the seasonal and geographical variability in tropospheric ozone, stratospheric  
790 influence and recent changes, *Atmospheric Chemistry and Physics*, 19(6), 3589–3620,  
791 doi:10.5194/acp-19-3589-2019, 2019.

792 World Meteorological Organization (1957). *Meteorology—A three dimensional science: Second*  
793 *session of the Commission for Aerology*. WMO Bulletin, IV(4), 134–138.

794 Xia, Y., Xie, F. and Lu, X.: Enhancement of Arctic surface ozone during the 2020–2021 winter  
795 associated with the sudden stratospheric warming, *Environmental Research Letters*, 18(2),  
796 024003, doi:10.1088/1748-9326/acace0, 2023.

797 Xia, Y., Huang, Y. and Hu, Y.: On the climate impacts of upper tropospheric and lower  
798 stratospheric ozone, *Journal of Geophysical Research: Atmospheres*, 123(2), 730–739,  
799 doi:10.1002/2017jd027398, 2018.

800 Zhang, J., Zhang, C., Zhang, K., Xu, M., Duan, J., Chipperfield, M. P., Feng, W., Zhao, S., and  
801 Xie, F.: The role of chemical processes in the quasi-biennial oscillation (QBO) signal in  
802 stratospheric ozone, *Atmospheric Environment*, 244, 117906,  
803 <https://doi.org/10.1016/j.atmosenv.2020.117906>, 2020.

804 Ziemke, J. R., Chandra, S. and Bhartia, P. K.: “cloud slicing”: A new technique to derive upper  
805 tropospheric ozone from satellite measurements, *Journal of Geophysical Research:*  
806 *Atmospheres*, 106(D9), 9853–9867, doi:10.1029/2000jd900768, 2001.

807